Two-Dimensional CS Adaptive FIR Wiener Filtering Algorithm for the Denoising of Satellite Images

Shilpa Suresh, *Student Member, IEEE*, and Shyam Lal, *Member, IEEE*

***Abstract*—In the recent years, researchers are quite much attracted in designing two-dimensional (2-D) adaptive finite-impulse response (FIR) filters driven by an optimization algorithm to self-adjust the filter coefficients, with applications in different domains of research. For signal processing applications, FIR Wiener filters are commonly used for noisy signal restorations by computing the statistical estimates of the unknown signal. In this paper, a novel 2-D Cuckoo search adaptive Wiener filtering algorithm (2D-CSAWF) is proposed for the denoising of satellite images contaminated with Gaussian noise. Till date, study based on 2-D adaptive Wiener filtering driven by metaheuristic algorithms was not found in the literature to the best of our knowledge. Comparisons are made with the most studied and recent 2-D adaptive noise filtering algorithms, so as to analyze the performance and computational efficiency of the proposed algorithm. We have also included comparisons with recent adaptive metaheuristic algorithms used for satellite image denoising to ensure a fair comparison. All the algorithms are tested on the same satellite image dataset, for denoising images corrupted with three different Gaussian noise variance levels. The experimental results reveal that the proposed novel 2D-CSAWF algorithm outperforms others both quantitatively and qualitatively. Investigations were also carried out to examine the stability and computational efficiency of the proposed algorithm in denoising satellite images.**

***Index Terms*—Adaptive filter algorithm, cuckoo search (CS) algorithm, metaheuristic optimization algorithms, satellite image denoising, two-dimensional finite-impulse response (2-D FIR) Wiener filter.**

I. Introduction

Satellite images are the only source available and exploited for applications, such as astronomy, geographical information system, and geoscience studies, for future decision making. Due to wrong ISO settings, sensor imperfections, defects in transmission channels together with physical constraints, the quality of such acquired satellite images gets deteriorated [1]. Hence, denoising such images has become a prior essential step for satellite image processing and analysis applications. Later, several classes of denoising algorithms, such as wavelets [2]–[6], nonlocal means [7], total variation (TV) [8], and few more [9], [10], were proposed. The wavelet-based denoising methods use the statistical features of the image coefficients. The nonlocal means denoising methods make use of image texture feature redundancy. Whereas, the TV-based methods extract the geometric features of the image for performing image denoising. Several other methods also evolved specifically for the denoising of satellite images corrupted with various types of noises [7], [9]–[14]. Although these methods resulted in fairly good overall performance, the main challenge in satellite image denoising was to devise an efficient way to preserve the structures bearing relevant informations like edges and textures, ensuring satisfactory visual quality.

Meanwhile, approaches for designing two-dimensional (2-D) digital filters attracted the attention of researchers and practitioners. Numerous studies related to adaptive filters have been propounded in various research areas for noise cancellation and image deblurring, till date, [15], [16]. The least mean square (LMS) filter was first in the row to get modified to use for 2-D adaptive filtering [17], [18]. The 2-D normalized LMS (NLMS) was introduced later to overcome the low convergence speed of the aforementioned LMS algorithm. Eventually, algorithms like 2-D affine projection algorithms (2D-APA) also evolved ensuring fast convergence rate and better observation capability [19]–[21]. Similarly, 2-D adaptive finite-impulse response (FIR) Wiener filters were proposed, which resulted in an optimal trade-off between inverse filtering and noise smoothing [22]. The filter coefficients of these 2-D adaptive filters were optimized at each iteration using conventional optimization algorithms.

Recently, evolutionary and swarm intelligence based algorithms have been widely used for image denoising [11], [23], [24] and for designing adaptive 2-D FIR digital filters [25]–[27]. For instance, Tzeng proposed a design for a 2-D FIR digital filter using a genetic algorithm [25]. An extensive comparative study on evolutionary algorithms for designing 2-D FIR digital filters was done by Boudjelaba *et al.* [26]. Latifoglu proposed a novel filtering approach for denoising medical images corrupted with speckle noise based on artificial bee colony (ABC) algorithm [28]. In 2014, Sarangi *et al.* designed 1-D and 2-D recursive filters using crossover bacterial foraging and Cuckoo search (CS) techniques [27]. Kockanat *et al.* proposed a 2-D FIR filtering approach using the ABC algorithm for denosing natural images [29]. Later, Kockanat and Karaboga reframed the framework for designing an adaptive FIR filter for noise cancellation applications, which optimized the filter coefficients using the ABC algorithm [30]. In this paper, a novel 2D-CS adaptive Wiener filtering algorithm (2D-CSAWF) is proposed for the denoising of satellite images corrupted with additive white Gaussian noise.

Manuscript received March 10, 2017; revised June 15, 2017; accepted September 7, 2017. Date of publication October 29, 2017; date of current version November 27, 2017. *(Corresponding author: Shyam Lal.)*

The authors are with the Department of Electronics and Communication Engineering, National Institute of Technology Karnataka, Mangaluru 575025, India (e-mail: shilparagesh89@gmail.com; shyam.mtec@gmail.com).

Color versions of one or more of the figures in this paper are available online at http://ieeexplore.ieee.org.

Digital Object Identifier 10.1109/JSTARS.2017.2755068

1939-1404 © 2017 IEEE. Personal use is permitted, but republication/redistribution requires IEEE permission.
See http://www.ieee.org/publications_standards/publications/rights/index.html for more information.

The major contributions of this paper are the following.

1) A metaheuristic-based adaptive Wiener filtering algorithm for image denoising is proposed for the first time in the literature, to the best of our knowledge.
2) Significant reduction in the computational complexity compared with the state-of-the-art algorithms, since it does not require the transformation of signals into any complex domain.
3) Substantial improvement in the quantitative and qualitative metric values for all noise variance levels computed, compared with aforementioned algorithms.
4) Stability in performance making it adaptable for other real-time signal processing applications.

The rest of this paper is structured as follows. Section II includes the basic analysis of 2-D FIR Wiener filters used in our study. Section III presents a detailed discussion about the proposed 2D-CSAWF algorithm for denoising satellite images. Results and discussions are included in Section IV. Section V concludes the discussion emphasizing the significance of the proposed algorithm.

II. 2-D FIR Wiener Filtering

This section presents the theory and fundamental concepts of 2-D adaptive FIR Wiener filtering method used for denoising satellite images in the proposed algorithm. In the literature, 2-D FIR Wiener filters have been used for applications like signal restoration, system identification, linear prediction, echo cancellation, and channel equalization. Wiener filter coefficients are evaluated to minimize the mean squared error (MSE) between the desired signal and the filter signal estimate. The signals are assumed to be stationary according to the theory of Wiener filtering [31]. For 2-D Wiener filtering, the coefficients are calculated periodically for a block of $n \times n$ samples, which will eventually adapt the filter with the average signal characteristics of the block, making it block adaptive. Hence, for relatively small block of samples, a block adaptive Wiener filter can be considered almost stationary. Therefore, the key objective of the 2-D adaptive FIR Wiener filter is the restoration of the image by minimizing the MSE value, which can be achieved using an efficient optimization algorithm.

To model an adaptive Wiener filter for image denoising, consider the simple scenario of filtering a noisy image, $y_{(i,j)}$, which is corrupted by signal-independent additive white Gaussian noise $\eta_{(i,j)}$. This can be mathematically formulated as follows:

$$y_{(i,j)} = x_{(i,j)} + \eta_{(i,j)}. \tag{1}$$

The requirement is to remove noise from $y_{(i,j)}$ to obtain a linear estimate $\hat{x}_{(i,j)}$ of original input signal $x_{(i,j)}$ by minimizing the MSE as given in the following equation:

$$\text{MSE}(\hat{x}) = \sum_{i=1}^{M}\sum_{j=1}^{N}\left[\hat{x}_{(i,j)} - x_{(i,j)}\right]^2 \tag{2}$$

where $[M, N]$ denotes the dimensionality of the input image. Considering the input $x_{(i,j)}$ also to be a white Gaussian process, the linear estimate $\hat{x}_{(i,j)}$ using the Wiener filter can be represented as a simple scalar form as [32], [33]

$$\hat{x}_{(i,j)} = \frac{\sigma^2_{x_{(i,j)}}}{\sigma^2_{x_{(i,j)}} + \sigma^2_{\eta_{(i,j)}}}\left[y_{(i,j)} - \mu_{x_{(i,j)}}\right] + \mu_{x_{(i,j)}} \tag{3}$$

where μ and σ^2 indicates the signal mean and variance, respectively, assuming the noise mean to be zero.

Assuming noise mean $\mu_{\eta_{(i,j)}}$ and variance $\sigma^2_{\eta_{(i,j)}}$ to be known, we focus on estimating $\mu_{x_{(i,j)}}$ and $\sigma^2_{x_{(i,j)}}$ [34], [35]. Generally, the calculation of local mean and variance includes the use of a moving average window of dimension size $(2n+1) \times (2n+1)$ as given in the following equation [32]:

$$\begin{aligned}\hat{\mu}_{x_{(i,j)}} &= \frac{1}{(2n+1)^2}\sum_{p=i-n}^{i+n}\sum_{q=j-n}^{j+n} y_{(p,q)}\\ \hat{\sigma}^2_{x_{(i,j)}} &= \frac{1}{(2n+1)^2}\sum_{p=i-n}^{i+n}\sum_{q=j-n}^{j+n}\left[y_{(p,q)} - \hat{\mu}_{x_{(i,j)}}\right]^2 - \sigma^2_{\eta}.\end{aligned} \tag{4}$$

However, the use of this local linear minimum MSE (LLMMSE) filter introduces blurring around the edges, because of the assumption that all the samples within the selected window falls in the same ensemble, which make the image appear noisy [32]. To overcome this ill-effect, Kuan *et al.* introduced a weighted form of computing local signal variance without modifying the local mean calculation as used in LLMMSE filtering [33]. It is mathematically modeled as in (5), wherein, the authors suggested the use of a monotonically decreasing function like Gaussian to calculate the weights $w_{(i,j,p,q)}$, by imposing more confidence on variance estimate at the center of the window

$$\hat{\sigma}^2_{x_{(i,j)}} = \sum_{p=i-n}^{i+n}\sum_{q=j-n}^{j+n}\left[w_{(i,j,p,q)}\left(y_{(p,q)} - \hat{\mu}_{x_{(i,j)}}\right)\right]^2. \tag{5}$$

The use of an adaptive weight factor, rather than using a deterministic weight as propounded by Kuan *et al.*, seems to be more reliable and appropriate [33]. Hence, in our proposed algorithm, the Wiener weights are adaptively improved by using a well-known metaheuristic approach, called CS [36], with an objective of reducing the MSE between the desired signal and the filter signal estimate. This adaptive weight $w_{(.)}$ is then used for estimating both local mean and variance, as given in (6), which eventually helps in denoising the input noisy image to its best possible extend

$$\begin{aligned}\hat{\mu}_{x_{(i,j)}} &= \sum_{p=i-n}^{i+n}\sum_{q=j-n}^{j+n} w_{(i,j,p,q)}y_{(p,q)}\\ \hat{\sigma}^2_{x_{(i,j)}} &= \sum_{p=i-n}^{i+n}\sum_{q=j-n}^{j+n}\left[w_{(i,j,p,q)}\left(y_{(p,q)} - \hat{\mu}_{x_{(i,j)}}\right)\right]^2.\end{aligned} \tag{6}$$

III. Proposed 2D-CSAWF Algorithm

The CS algorithm developed by Yang and Deb followed three major idealized rules in its run, which are enumerated as follows.

1) A single egg is laid by each cuckoo in a randomly selected nest.

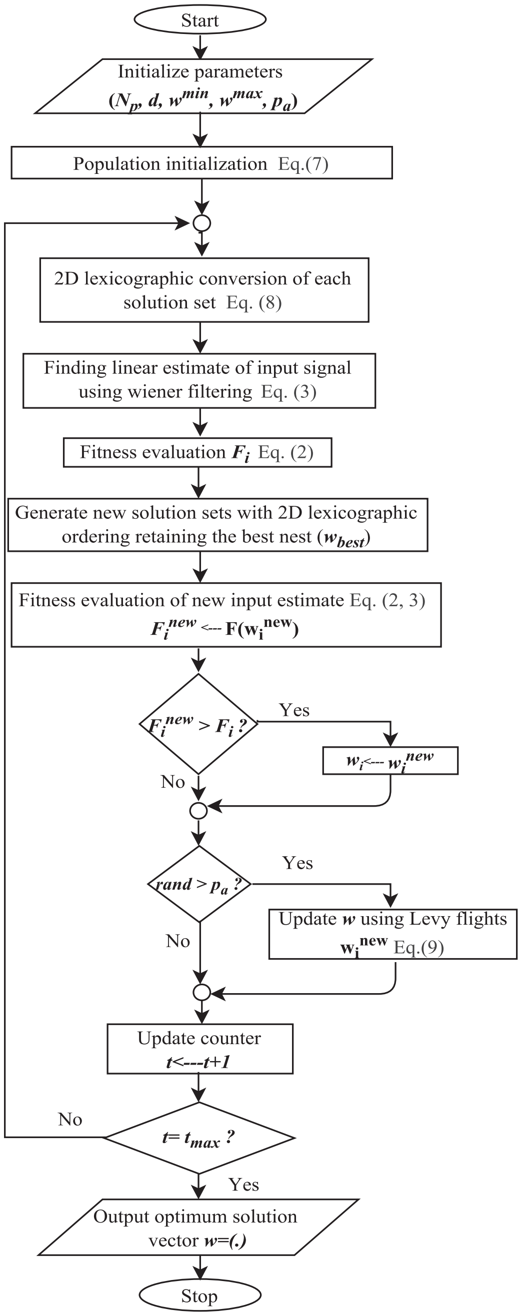

Fig. 1. Flowchart of the proposed 2D-CSAWF algorithm.

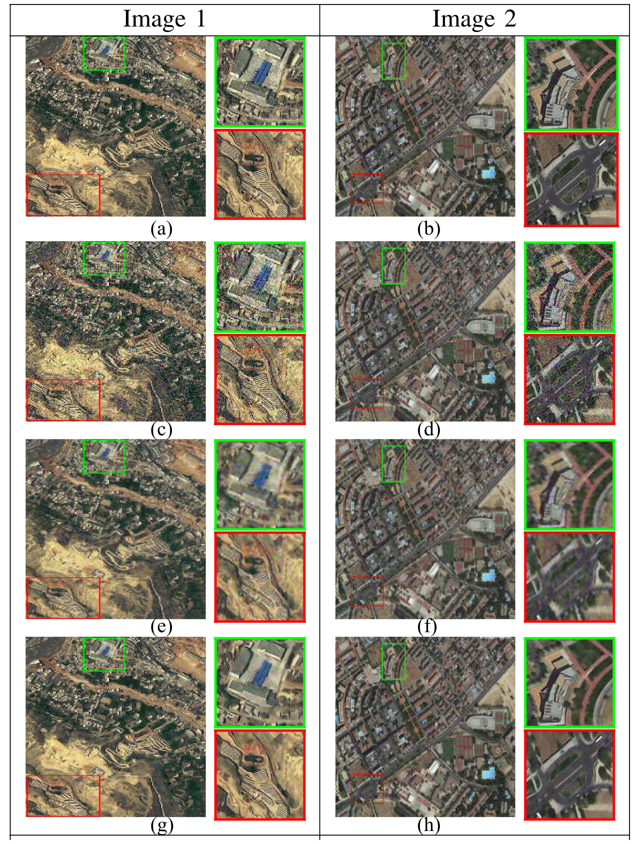

Fig. 2. Experimental results of denoising images using 2D-AWF and 2D-CSAWF algorithms for 30% noise variance level: (a) and (e) original images, (b) and (f) noisy images, (c) and (g) denoised images using 2D-AWF, (d) and (h) denoised images using 2D-CSAWF.

TABLE I
QUANTITATIVE RESULT COMPARISON BETWEEN 2D-AWF (WITHOUT CS) AND PROPOSED 2D-CSAWF ALGORITHMS FOR IMAGE 1 AND IMAGE 2 WITH THREE DIFFERENT NOISE VARIANCE LEVELS

σ^2	Met. \ Algo.	2D-AWF	2D-CSAWF	2D-AWF	2D-CSAWF
		Image 1		Image 2	
10%	MSE	222.8147	**128.4861**	217.2714	**209.313**
	PSNR	24.6514	**27.0422**	24.7608	**24.9228**
	FSIM	0.9668	**0.9756**	0.9776	**0.9776**
	UQI	0.9903	**0.9984**	0.9021	**0.9498**
	NAE	0.1443	**0.1014**	0.1961	**0.1924**
	Time (s)	7.77	7.56	7.03	7.92
20%	MSE	255.5587	**137.303**	340.1693	**232.4691**
	PSNR	24.0559	**26.754**	22.8139	**24.4672**
	FSIM	0.944	**0.9696**	0.9599	**0.9716**
	UQI	0.9901	**0.9984**	0.8841	**0.9452**
	NAE	0.1542	**0.1021**	0.2455	**0.1964**
	Time (s)	8.99	9.436	8.973	9.102
30%	MSE	345.7862	**137.6731**	376.9581	**232.0443**
	PSNR	22.7427	**26.7423**	22.3679	**24.4751**
	FSIM	0.9324	**0.9695**	0.9478	**0.9717**
	UQI	0.9846	**0.9983**	0.875	**0.9179**
	NAE	0.2123	**0.1022**	0.2653	**0.1963**
	Time (s)	11.986	12.586	13.101	13.426

The bold values indicate the best results for each performance metric compared.

2) The most potent nests with the high-quality eggs evolve by carrying over to the forthcoming generation.
3) The total number of nests is considered to be fixed in a scenario [36].

The CS algorithm has been adopted in the modeling proposed denoising algorithm, owing to its improved performance in solving nonlinear optimization problems based on a prior analytical study [37], [38]. The simplicity of its implementations accounts for the fact that it depends only on a single control parameter p_a. The switching parameter p_a denotes the probability of discovery of cuckoo's eggs by the host species. This is implemented by replacing p_a proportion of the eggs by new eggs in each iteration to obtain more potential solution, which in turn controls the balance combination of local (exploitation) and global random walks (exploration) of the optimization algorithm. The CS algorithm also exploits Lévy flight strategy rather than Brownian random walks as in other nature inspired

TABLE II
PERFORMANCE METRICS COMPARISON OF DIFFERENT DENOISING ALGORITHMS FOR IMAGE 1 (HTTP://EARTHOBSERVATORY.NASA.GOVX, WORLDVIEW-2, MS 50 M, LANDSLIDE IN ZHOUQU, CHINA, 1263 × 1261) WITH THREE DIFFERENT NOISE VARIANCE LEVELS

σ^2	Met. \ Algo.	**2D-LMS**	**2D-NLMS**	**2D-APA**	**PDE-AIP**	**CII-NLM**	**DST**	**SSTV**	**2D-ABC**	**JADE**	**2D-CSAWF**
10%	MSE	138.3885	138.1648	176.9961	261.0002	271.2083	288.3612	168.913	176.0388	196.0059	**128.4861**
	PSNR	26.7198	26.7268	25.6512	23.9644	23.7978	23.5314	25.8542	25.6747	25.2081	**27.0422**
	FSIM	0.9695	0.9691	0.9711	0.9725	0.9719	0.9727	0.9668	0.9718	0.9693	**0.9756**
	UQI	0.9984	0.9983	0.998	0.9977	0.9966	0.9974	0.9983	0.9979	0.9967	**0.9984**
	NAE	0.1023	0.1024	0.1229	0.1253	0.1381	0.1368	0.1143	0.1176	0.125	**0.1014**
	Time (s)	8.561	9.469	18.452	22.392	9.613	10.113	14.556	16.252	12.543	**7.56**
20%	MSE	197.6974	251.6535	195.4102	362.1446	480.2542	326.901	217.7484	230.8015	244.4655	**137.303**
	PSNR	25.1708	24.1228	25.2213	22.542	21.3161	22.9866	24.7513	24.4984	24.2486	**26.754**
	FSIM	0.9522	0.9559	0.9598	0.9671	0.9569	0.9594	0.954	0.9577	0.953	**0.9696**
	UQI	0.9972	0.9966	0.9969	0.9954	0.9976	0.9954	0.9969	0.9967	0.9965	**0.9984**
	NAE	0.1228	0.1422	0.1303	0.1506	0.1056	0.1418	0.1306	0.1374	0.1391	**0.1021**
	Time (s)	9.421	10.991	22.434	24.634	10.715	12.339	16.773	20.333	16.543	**9.436**
30%	MSE	245.5038	368.1637	261.7553	477.7469	690.315	425.4046	255.4553	277.3758	450.2817	**137.6731**
	PSNR	24.2302	22.4704	23.9518	21.3388	19.7403	21.8428	24.0577	23.7001	21.596	**26.7423**
	FSIM	0.9388	0.9378	0.9454	0.9692	0.9642	0.9606	0.9446	0.9445	0.9315	**0.9695**
	UQI	0.9959	0.9857	0.9951	0.9938	0.9967	0.9932	0.9953	0.9953	0.9553	**0.9983**
	NAE	0.1374	0.1772	0.1521	0.1748	0.1076	0.1587	0.1434	0.1523	0.1996	**0.1022**
	Time (s)	10.245	11.456	26.114	28.315	11.663	13.55	18.991	22.233	29.772	**12.586**

The bold values indicate the best results for each performance metric compared.

TABLE III
PERFORMANCE METRICS COMPARISON OF DIFFERENT DENOISING ALGORITHMS FOR IMAGE 2 (WWW.SATIMAGINGCORP.COM, WORLDVIEW-3, MS 40 CM, MADRID, SPAIN, 1000 × 1000) WITH THREE DIFFERENT NOISE VARIANCE LEVELS

σ^2	Met. \ Algo.	**2D-LMS**	**2D-NLMS**	**2D-APA**	**PDE-AIP**	**CII-NLM**	**DST**	**SSTV**	**2D-ABC**	**JADE**	**2D-CSAWF**
10%	MSE	232.4294	231.7467	230.6078	239.5899	252.4129	280.3517	274.178	217.3529	237.0807	**209.313**
	PSNR	24.4679	24.4807	24.5021	24.3361	24.1097	23.6538	23.7505	24.7591	24.3818	**24.9228**
	FSIM	0.9714	0.9714	0.9765	0.9741	0.9773	0.9763	0.9716	0.977	0.9764	**0.9776**
	UQI	0.9254	0.9392	0.9084	0.9081	0.9391	0.9383	0.9301	0.9034	0.9188	**0.9498**
	NAE	0.1965	0.1962	0.2016	0.1927	0.1965	0.1968	0.2168	0.1959	0.1955	**0.1924**
	Time (s)	7.571	9.554	20.554	23.335	10.331	11.432	14.996	17.801	14.893	**7.92**
20%	MSE	320.4456	340.9504	287.5738	341.2975	460.8813	302.2861	336.2252	308.0926	384.2303	**232.4691**
	PSNR	23.0733	22.8039	23.5433	22.7995	21.4949	23.3266	22.8645	23.244	22.2849	**24.4672**
	FSIM	0.955	0.9547	0.9623	0.9705	0.9652	0.9661	0.9584	0.961	0.9574	**0.9716**
	UQI	0.9008	0.8787	0.8864	0.9167	0.9412	0.9268	0.8823	0.8947	0.86	**0.9452**
	NAE	0.2368	0.2479	0.2313	0.1978	0.1995	0.2004	0.2464	0.2356	0.2569	**0.1964**
	Time (s)	9.486	11.452	22.486	25.689	11.332	12.316	15.335	18.423	16.584	**9.102**
30%	MSE	385.856	376.0204	366.7047	456.3029	670.3104	387.6814	385.2724	374.6892	647.4976	**232.0443**
	PSNR	22.2666	22.3787	22.4876	21.5383	19.868	22.2461	22.2731	22.3941	20.0184	**24.4751**
	FSIM	0.941	0.9461	0.9492	0.9641	0.9689	0.9661	0.9478	0.9465	0.938	**0.9717**
	UQI	0.8784	0.8807	0.8693	0.8955	0.9114	0.8952	0.8705	0.8792	0.7248	**0.9179**
	NAE	0.2647	0.265	0.2648	0.1997	0.1993	0.2021	0.2692	0.2628	0.3403	**0.1963**
	Time (s)	12.2546	13.452	25.842	26.991	12.335	14.603	16.781	22.548	28.563	**13.426**

The bold values indicate the best results for each performance metric compared.

TABLE IV
PERFORMANCE METRICS COMPARISON OF DIFFERENT DENOISING ALGORITHMS FOR IMAGE 3 (WWW.SATIMAGINGCORP.COM, WORLDVIEW-3, MS 0.31 CM, RAINBOW RANGE, BRITISH COLUMBIA, 1600 × 1200) WITH THREE DIFFERENT NOISE VARIANCE LEVELS

σ^2	Met. \ Algo.	**2D-LMS**	**2D-NLMS**	**2D-APA**	**PDE-AIP**	**CII-NLM**	**DST**	**SSTV**	**2D-ABC**	**JADE**	**2D-CSAWF**
10%	MSE	187.825	188.0548	222.8147	223.1842	169.5154	231.0159	239.59	201.246	604.0624	**170.8726**
	PSNR	25.3933	25.388	24.6514	24.6442	25.8387	24.4944	24.3361	25.0935	20.32	**25.8041**
	FSIM	0.984	0.9843	0.9819	0.9478	0.9781	0.9516	0.9824	0.9862	0.9589	**0.9873**
	UQI	0.9854	0.9853	0.9501	0.993	0.9923	0.994	0.9948	0.9949	0.8231	**0.995**
	NAE	0.1331	0.1332	0.1465	0.1763	0.1993	0.199	0.1517	0.1385	0.2553	**0.1299**
	Time (s)	9.456	10.596	17.895	20.456	10.564	11.462	15.156	17.523	13.985	**8.356**
20%	MSE	255.5587	266.8165	236.8207	238.3827	386.2833	193.5236	287.0196	265.9157	327.8638	**187.7084**
	PSNR	24.0559	23.8687	24.3866	24.3581	22.2617	25.2635	23.5517	23.8834	22.9739	**25.396**
	FSIM	0.9742	0.9766	0.9784	0.9217	0.9231	0.9268	0.9744	0.9772	0.9733	**0.9844**
	UQI	0.9927	0.9902	0.9903	0.9946	0.9942	0.9938	0.9894	0.9905	0.9716	**0.9955**
	NAE	0.1558	0.1625	0.1545	0.1507	0.1977	0.1884	0.1667	0.1612	0.1794	**0.133**
	Time (s)	10.553	11.473	21.896	25.846	11.523	13.856	14.896	22.503	18.452	**10.236**
30%	MSE	309.1488	366.5373	303.5171	350.7489	601.7315	238.3689	321.0927	325.2051	395.9768	**187.9139**
	PSNR	23.2291	22.4896	23.309	22.6808	20.3368	24.3583	23.0645	23.0092	22.1541	**25.3912**
	FSIM	0.9652	0.9636	0.9694	0.8999	0.9758	0.8895	0.9674	0.9662	0.9643	**0.9844**
	UQI	0.9868	0.9873	0.9849	0.9921	0.9947	0.9904	0.9843	0.9876	0.9787	**0.9955**
	NAE	0.1724	0.1882	0.1761	0.153	0.1405	0.1965	0.1777	0.1791	0.1954	**0.1331**
	Time (s)	13.564	14.561	25.464	28.884	13.564	14.654	19.856	23.462	29.451	**12.998**

The bold values indicate the best results for each performance metric compared.

TABLE V

PERFORMANCE METRICS COMPARISON OF DIFFERENT DENOISING ALGORITHMS FOR IMAGE 4 (WWW.SATIMAGINGCORP.COM,SPOT, MS 0.31 CM, BRISBANE, AUSTRALIA, 2000 × 2542) WITH THREE DIFFERENT NOISE VARIANCE LEVELS

σ^2	Met. \ Algo.	2D-LMS	2D-NLMS	2D-APA	PDE-AIP	CII-NLM	DST	SSTV	2D-ABC	JADE	2D-CSAWF
10%	MSE	150.0014	150.2126	166.8924	162.198	185.0871	220.4531	180.3972	170.0101	263.0248	**134.3656**
	PSNR	26.3698	26.3637	25.9064	26.0303	25.457	24.6976	25.5685	25.8261	23.9308	**26.8479**
	FSIM	0.9299	0.929	0.9452	0.9455	0.9519	0.9502	0.9278	0.9467	0.939	**0.9528**
	UQI	0.994	0.9955	0.996	0.9965	0.9936	0.9956	0.995	0.9963	0.9504	**0.9966**
	NAE	0.0762	0.0762	0.0831	0.1156	0.1495	0.1451	0.0837	0.0822	0.1001	**0.0737**
	Time (s)	8.785	10.562	19.855	24.778	11.462	12.654	15.462	16.998	15.894	**8.234**
20%	MSE	202.4452	229.962	198.2046	254.7878	396.3217	195.5399	223.0803	224.7493	328.178	**149.5979**
	PSNR	25.0677	24.5142	25.1597	24.069	22.1503	25.2184	24.6462	24.6138	22.9697	**26.3815**
	FSIM	0.9063	0.9267	0.9287	0.9278	0.9223	0.9114	0.9145	0.925	0.91	**0.9289**
	UQI	0.9954	0.9948	0.9941	0.9952	0.9937	0.9962	0.9939	0.9945	0.9739	**0.9967**
	NAE	0.089	0.0984	0.091	0.1534	0.1296	0.1234	0.0936	0.0969	0.1166	**0.0761**
	Time (s)	10.564	12.564	23. 596	26.462	12.334	13.564	16.895	20.461	17.658	**10.004**
30%	MSE	243.7739	316.103	265.364	362.5804	599.9787	250.7325	257.3803	276.8505	392.6942	**149.8332**
	PSNR	24.2609	23.1325	23.8924	22.5368	20.3494	24.1387	24.0251	23.7083	22.1903	**26.3747**
	FSIM	0.8911	0.9041	0.9103	0.9232	0.9292	0.9163	0.9065	0.9066	0.8985	**0.9296**
	UQI	0.9928	0.9916	0.9917	0.993	0.9929	0.9936	0.9915	0.9925	0.9689	**0.9967**
	NAE	0.0981	0.116	0.1061	0.187	0.1283	0.1352	0.1015	0.1079	0.1306	**0.0762**
	Time (s)	11.561	13.654	26.541	26.998	13.345	15.246	17.989	23.564	29.453	**10.989**

The bold values indicate the best results for each performance metric compared.

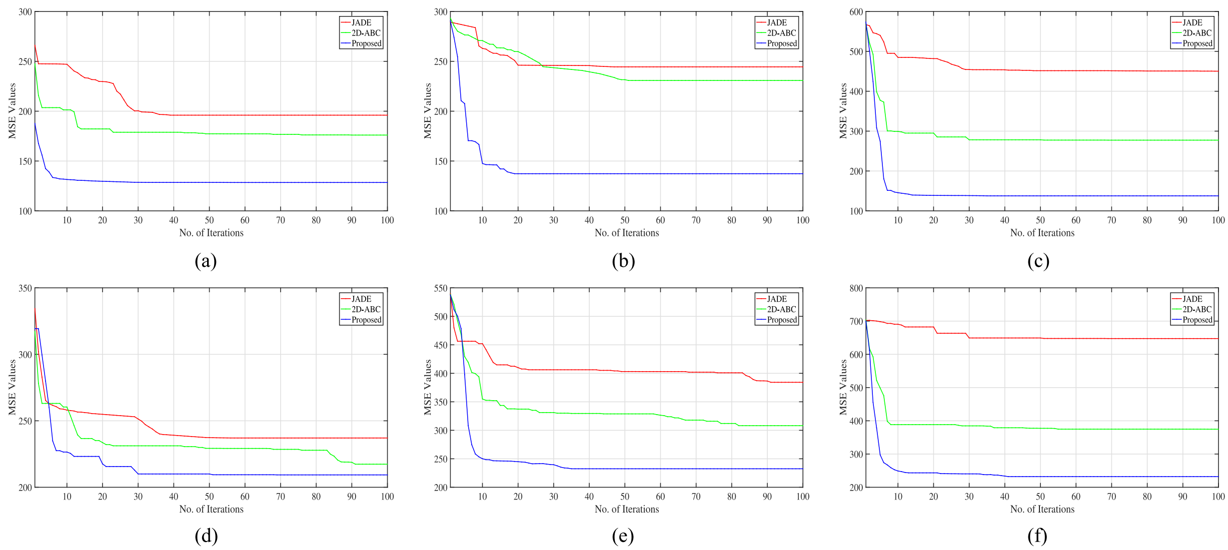

Fig. 3. Convergence rate analysis between JADE, 2D-ABC, and 2D-CSAWF algorithm. (a)–(c) the convergence plots for Image 1 for noise variance level of 10%, 20%, and 30%, respectively, and (d)–(f) similar plots for Image 2.

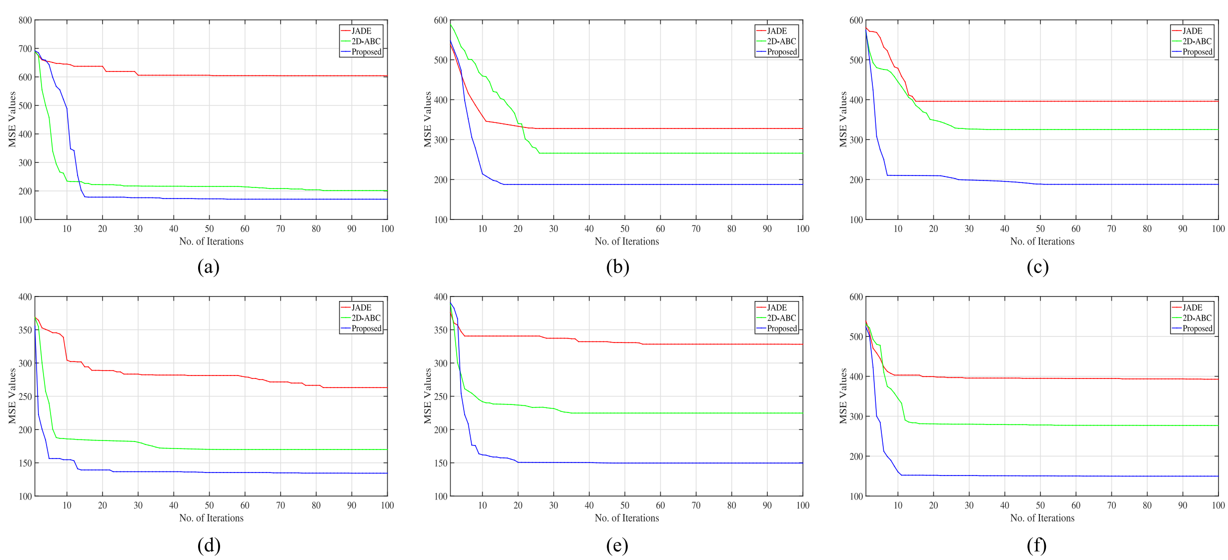

Fig. 4. Convergence rate analysis between JADE, 2D-ABC, and 2D-CSAWF algorithm. (a)–(c) the convergence plots for Image 3 for noise variance level of 10%, 20%, and 30%, respectively, and (d)–(f) similar plots for Image 4.

metaheuristic approaches, which indeed exhibits a fast convergence rate [36]. Implementation of our defined denoising scenario requires the optimization of the localized window weight factor $w_{(.)}$. This adaptive weight factor is optimized based on the MSE computed using (2).

The flowchart of the proposed 2D-CSAWF algorithm is shown in Fig. 1. The pseudocode of the 2D-CSAWF algorithm is given below.

Step 1: Initialize the population space comprising the weight matrix of 2-D FIR Wiener filter randomly $w_{i,j}$; $i = 1, ..., N_p; j = 1, ..., d$ (N_p: population size), ($d = n^2$: the number of the coefficients of 2-D FIR Wiener filter to form the weight matrix)

$$w_{i,j} = w_{i,j}^{\min} + \text{rand}(0,1)(w_{i,j}^{\max} - w_{i,j}^{\min}). \quad (7)$$

Step 2: Convert the weight matrix into their 2-D lexicographic form, as given in the following:

$$[w_{i,1}, w_{i,2}, w_{i,3}, ..., w_{i,n}, w_{i,n+1}, w_{i,n+2}, ..., w_{i,2n}, w_{i,n(n-1)+1} ... w_{i,d}] \Rightarrow \begin{bmatrix} w_{i,1} & \cdots & w_{i,n} \\ \cdots & \cdots & \cdots \\ w_{i,n(n-1)+1} & \cdots & w_{i,d} \end{bmatrix}. \quad (8)$$

Step 3: Evaluate $\hat{\mu}_{x_{(i,j)}}$ and $\hat{\sigma}^2_{x_{(i,j)}}$ using (6) to model the estimate $\hat{x}_{(i,j)}$ as given in (3) for the given noisy input image $y_{(i,j)}$

Step 4: Compute the fitness value of each possible weight matrix (nest) in the population using the objective function given in (2).

REPEAT if no. of iterations $t < t_{\max}$.

Step 5: Retain the best possible solution in the previous iteration and generate new random solutions for the other nests.

Step 6: Compute the fitness value of the newly generated solutions using (2).

Step 7: In each iteration, the probability of cuckoo's eggs being discovered by the host birds is given by the parameter p_a, and it is modeled by altering the solution space using Lévy flight using the following equation:

$$w_i(t+1) = w_i(t) + \alpha \oplus \text{Lévy}(\beta) \quad (9)$$

where α denotes the step size and $\text{Lévy}(\beta) = t^{-\beta}; 1 < \beta \leq 2$ which follows Lévy distribution [36].

Step 8: Evaluate the fitness value using (2) and record the best nest (weight vector) achieved so far.

Step 9: Increment the iteration by 1; t = t + 1.

UNTIL $t = t_{\max}$ *(maximum iterations).*

Step 10: Denoise $y_{(i,j)}$ using the optimal weight factor $w_{(.)}$ obtained to produce the best estimate of the input signal.

IV. Results and Discussion

The dataset used for simulation experiments includes satellite images obtained from different sources, such as NASA, Satpalda Geospatial Services, and Satellite Imaging Corp. Performance of the proposed 2D-CSAWF algorithm is compared with 2-D adaptive filtering techniques like 2D-LMS [17], [30], 2D-NLMS [30], [39], and 2D-APA [19], [30], since those are the most studied and compared algorithms in the literature. In addition to these, recent satellite image denoising algorithms using partial differential equations and auxiliary image priors (PDE-AIP) [2], nonlocal cosine integral images (CII-NLM) [7], discrete shearlet transform (DST) [10], and spatio-spectral TV (SSTV) [14] were also included for comparison. Furthermore, metaheuristics algorithms like JADE [13] and 2D-ABC adaptive filtering algorithm [30] were also used for the performance comparison to substantiate the efficiency. All the three stochastic metaheuristic algorithms were run for 31 independent trails, and the best results obtained are furnished. The simulation results obtained using four multispectral high spatial resolution satellite images are included in this section. All the algorithms were coded using MATLAB R2015a running on an Intel Core i7-3770 PC with 3.40-GHz CPU, 8-GB RAM, and 64-bit operating system.

Prior empirical study was undertaken to choose the optimal value for the single control parameter (p_a) used by the Wiener weight optimization algorithm, since it has a major impact on its performance [36], [37]. Thus, the value of the "switching parameter" p_a was chosen to be 0.5, which will set a decent tradeoff between the exploration and exploitation stages of the optimization algorithm (CS) used. The other parameters of the proposed algorithm, i.e., N_p, d, $w^{\min}$, $w^{\max}$, and $t_{\max}$ were chosen to be 50, 9 (for a window of size 3×3), -1, 1, and 100, respectively. The values for parameters used by other compared algorithm were adopted, as suggested by the authors in respective literatures.

The quantitative test parameters compared are MSE [40], peak signal-to-noise ratio (PSNR) [41], feature similarity index (FSIM) [42], universal quality index (UQI) [43], normalized absolute error (NAE) [44], and CPU running time. Fig. 2 and Table I give the qualitative and quantitative performance results obtained on denoising the test images with and without incorporating CS algorithm in 2-D adaptive FIR Wiener filtering.

It clearly proved the efficiency of the 2D-CSAWF algorithm in optimizing the wiener weights, which yielded improved qualitative and quantitative results, compared with the 2D-AWF. Table II–V present the values of the performance indicator parameters obtained by all the ten algorithms compared for Images 1, 2, 3, and 4 respectively. The MSE, NAE values, and CPU running time of the proposed denoising algorithm are comparatively low, and inversely PSNR, FSIM, and UQI values are significantly high for both test images, which gives a quantitative assessment about the improved performance of the proposed algorithm for the denoising of satellite images. The tables include the performance metric comparisons for three different noise variance level imposed on the input images (i.e., 10%, 20%, and 30%). Comparison of the values obtained in each of the three cases clearly indicated that the proposed algorithm is more stable and is well apt for denoising images with lower as well as higher noise levels.

Figs. 3 and 4 shows the convergence characteristics of the three metaheuristic-based algorithms (JADE, 2D-ABC, and 2D-CSAWF) used for comparison, the stopping criterion was

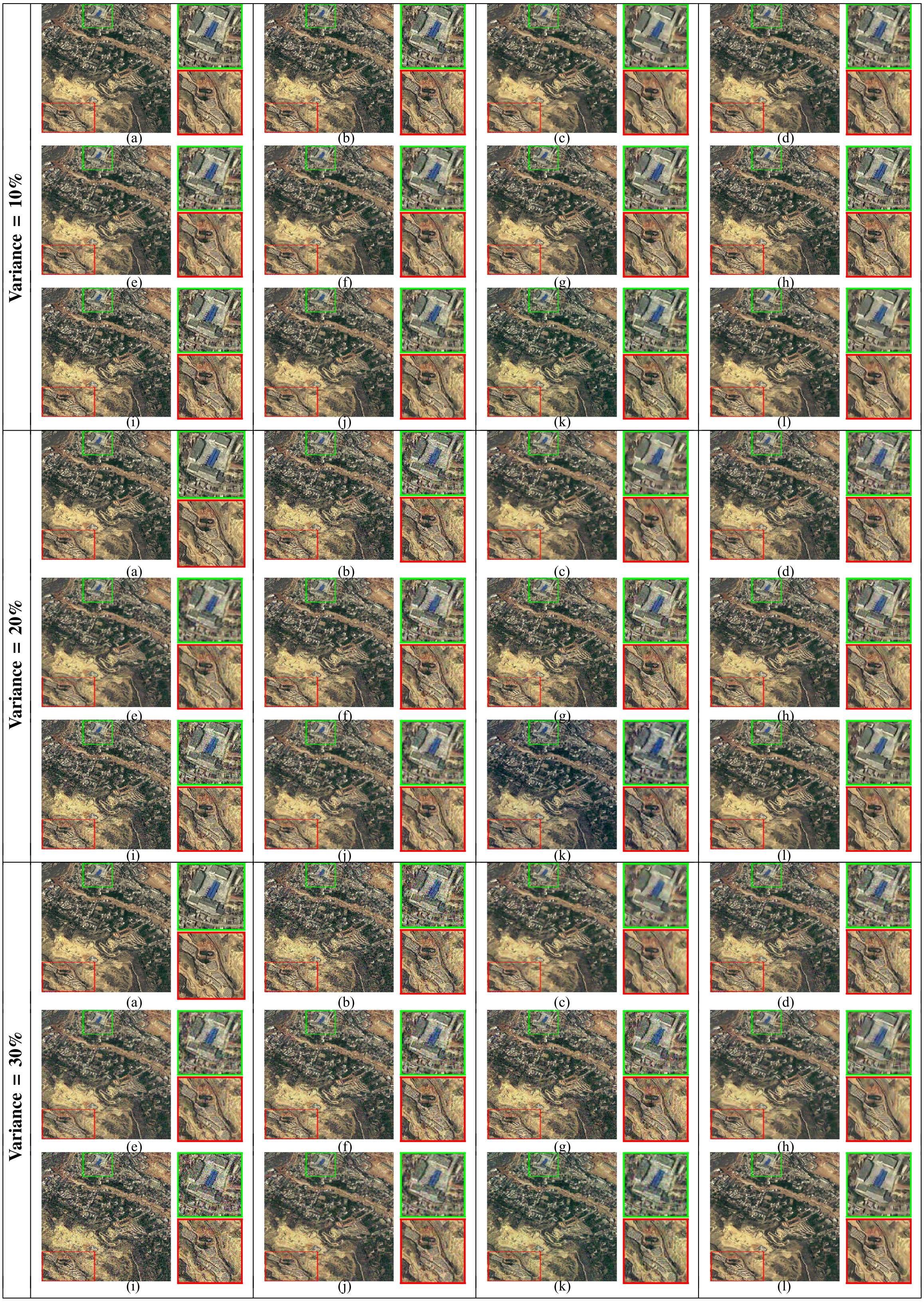

Fig. 5. Experimental results of denoising Image 1 using different algorithms for three different noise variance levels: (a) original, (b) noisy, (c) 2D-LMS, (d) 2D-NLMS, (e) 2D-APA, (f) PDE-AIP, (g) CII-NLM, (h) DST, (i) SSTV, (j) 2D-ABC adaptive filtering, (k) JADE, and (l) 2D-CSAWF.

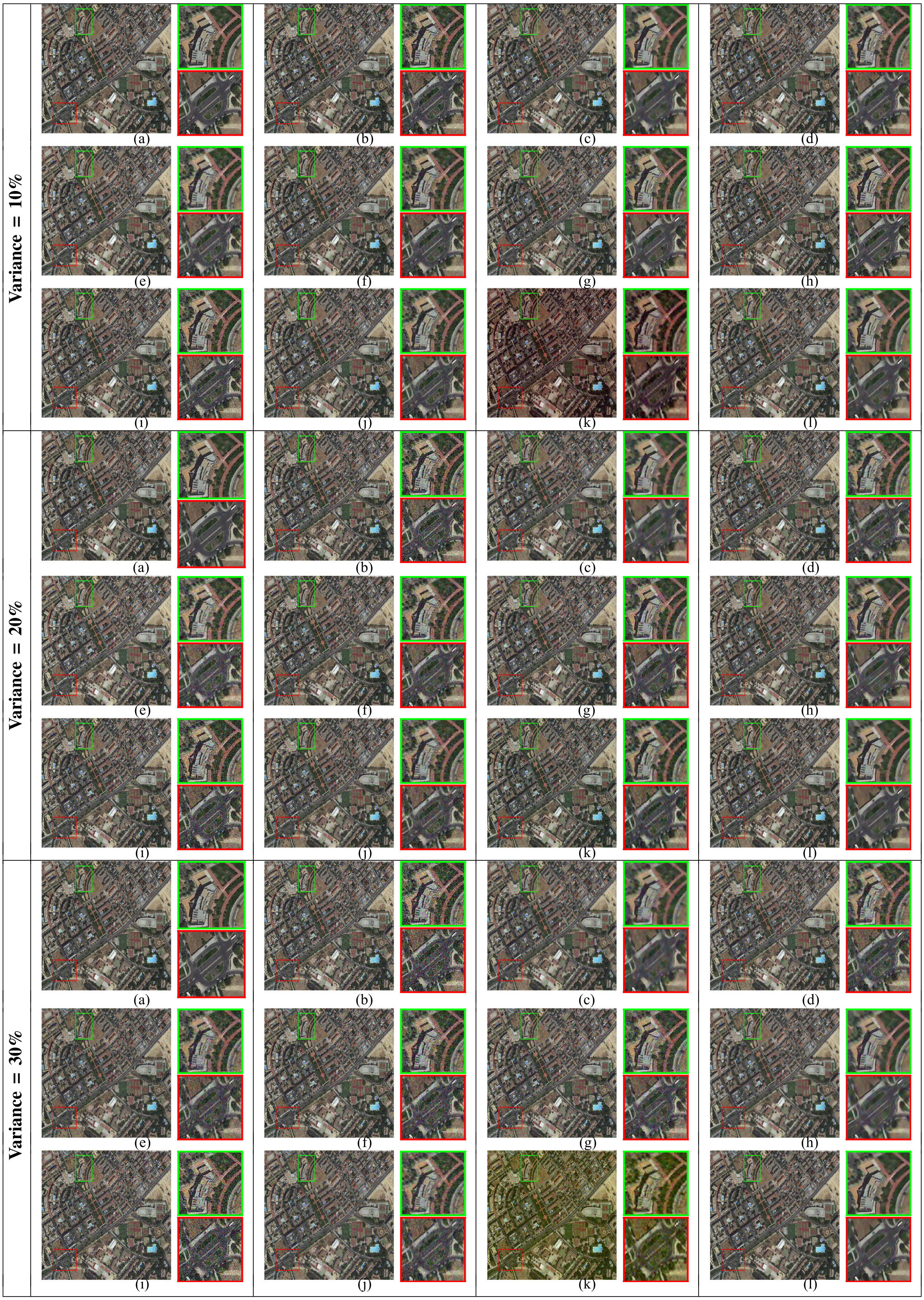

Fig. 6. Experimental results of denoising Image 2 using different algorithms for three different noise variance levels: (a) original, (b) noisy, (c) 2D-LMS, (d) 2D-NLMS, (e) 2D-APA, (f) PDE-AIP, (g) CII-NLM, (h) DST, (i) SSTV, (j) 2D-ABC adaptive filtering, (k) JADE, and (l) 2D-CSAWF.

Fig. 7. Experimental results of denoising Image 3 using different algorithms for three different noise variance levels: (a) original, (b) noisy, (c) 2D-LMS, (d) 2D-NLMS, (e) 2D-APA, (f) PDE-AIP, (g) CII-NLM, (h) DST, (i) SSTV, (j) 2D-ABC adaptive filtering, (k) JADE, and (l) 2D-CSAWF.

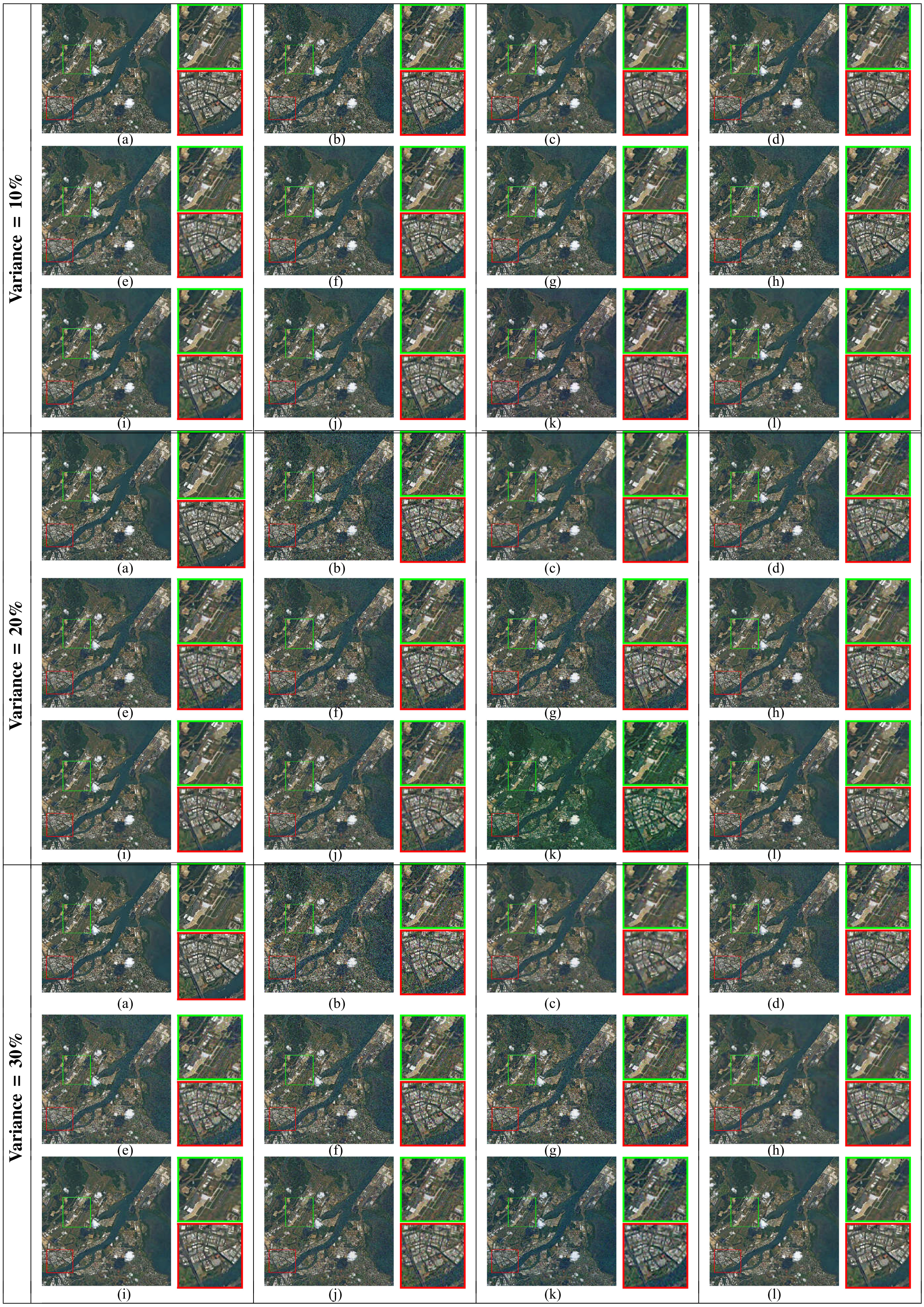

Fig. 8. Experimental results of denoising Image 4 using different algorithms for three different noise variance levels: (a) original, (b) noisy, (c) 2D-LMS, (d) 2D-NLMS, (e) 2D-APA, (f) PDE-AIP, (g) CII-NLM, (h) DST, (i) SSTV, (j) 2D-ABC adaptive filtering, (k) JADE, and (l) 2D-CSAWF.

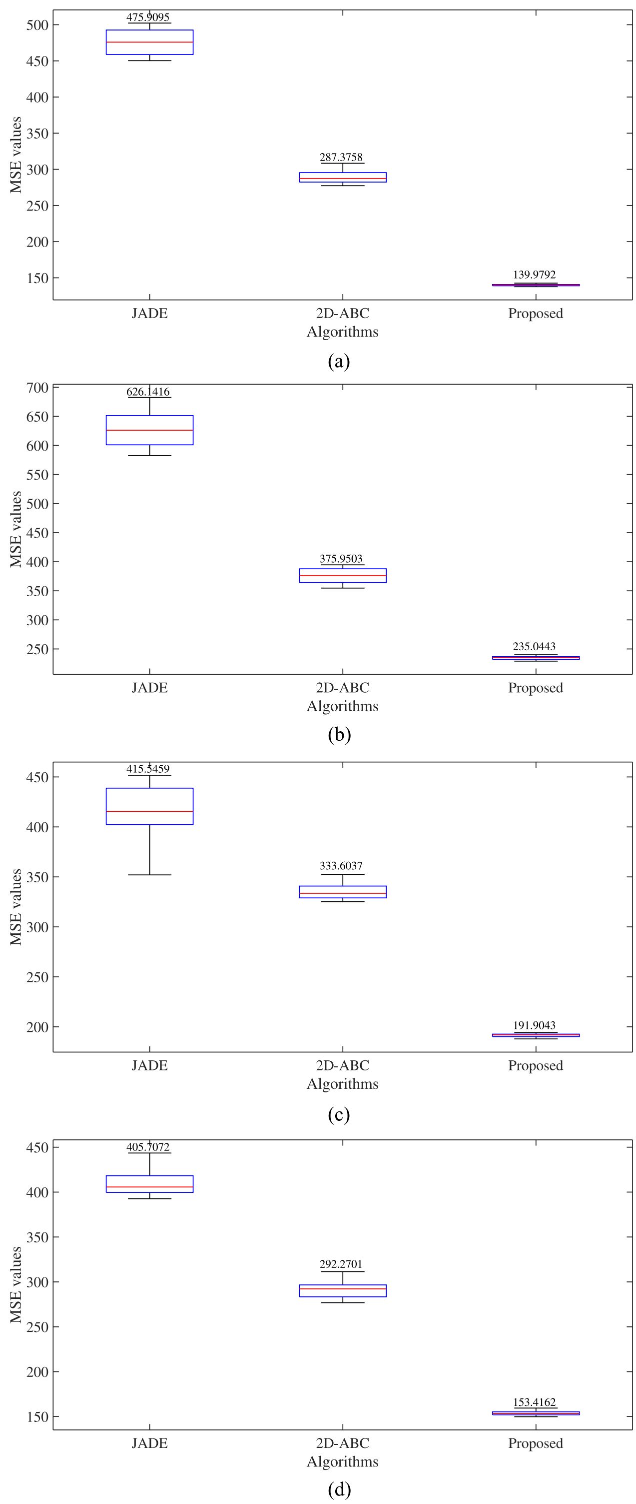

Fig. 9. Box plots comparing JADE, 2D-ABC, and 2D-CSAWF for test images: (a) Image 1, (b) Image 2, (c) Image 3, (d) Image 4 for 30% noise variance level.

established to 100 iterations. For all the test images, the 2D-CSAWF algorithm converges quickly and the MSE values approach to its lowest attainable limit. Hence, the rapid convergence ability of the proposed algorithm improves the computational efficiency reasonably making it adaptable for real-time applications. Figs. 5–8 includes the restored test images obtained

TABLE VI
STATISTICAL ANALYSIS OF JADE, 2D-ABC, AND 2D-CSAWF ALGORITHMS FOR DENOISING TEST IMAGES CORRUPTED WITH GAUSSIAN NOISE OF 30 % NOISE VARIANCE LEVEL

Image	Algorithm	STD	Mean	Best	Worst
1	JADE	17.579	473.5087	450.2817	502.2817
	2D-ABC	8.7461	289.599	277.3758	308.3758
	2D-CSAWF	**1.4043**	**140.1058**	**137.6731**	**142.6731**
2	JADE	29.0564	627.3001	582.4976	682.4976
	2D-ABC	12.7946	376.1842	354.6892	394.6892
	2D-CSAWF	**3.0652**	**234.4682**	**229.0443**	**240.0443**
3	JADE	22.2418	418.867	352	451.7078
	2D-ABC	6.98	334.8134	325.2051	352.4595
	2D-CSAWF	**1.6656**	**191.5681**	**187.9139**	**194.2211**
4	JADE	11.7775	409.2593	392.6942	443.541
	2D-ABC	9.031	291.1749	276.8505	311.4554
	2D-CSAWF	**2.1391**	**153.5969**	**149.8332**	**159.4545**

The bold values indicate the best results for each performance metric compared.

using different denoising algorithms compared. The qualitative comparison revealed that the filtered output images obtained using the proposed 2D-CSAWF algorithm resulted in a better visual quality as compared with other existing denoising algorithms. It also resulted in a much smoother denoised images, preserving significant edges and other textural features. It even proved to produce very less image blurring for all three noise variance levels tested in terms of feature visibility. This makes the proposed algorithm well adaptable to be used in the preprocessing stages of further satellite image processing applications.

Box-and-whisker plots are commonly used to estimate the converging capability and stability of algorithms to reach its global optimum solutions in fixed number of iterations. The random population initialization phase followed by the solution tracking capability framed by the specific exploration and exploitation stages of the optimization algorithm, have a major impact in controlling its convergence characteristics. Hence, the stability of a metaheuristic-based algorithm accounts for the repeatability of the same under the similar constraints over time, which is of great importance for all real-time applications. Fig. 9. includes the box-and-whisker plots for the three metaheuristic-based denoising algorithms, i.e., JADE, 2D-ABC, and the 2D-CSAWF, included in our study after 31 independent trails, for all the test images. The median value is shown above the respective boxes, and is indicated by a red line across each box in the plot. Table VI presents the statistical analysis between JADE, 2D-ABC, and 2D-CSAWF algorithms, comparing the standard deviation, mean, best, and worst values of the defined fitness function (MSE) evaluated. It gives substantial evidence to prove the stability of the 2D-CSAWF algorithm, ensuring the LMSE value for all the test images.

V. CONCLUSION

In this paper, a 2D-CS adaptive FIR Wiener filtering algorithm was proposed for the denoising of satellite images. The CS algorithm was used to adaptively optimize the weights of a 2-D FIR Wiener filter for denoising test images. The novelty of the proposed algorithm accounts for the fact that a metaheuristic algorithm based adaptive Wiener filtering approach for image denoising is not studied in the literature till date, to the best of our knowledge. In order to demonstrate the performance efficiency of the proposed algorithm, it was tested for the denoising of satellite images taken from different image datasets. The algorithms used for performance comparison included the most studied and compared 2-D adaptive filtering algorithms like 2D-LMS, 2D-NLMS, and 2D-APA. Recent algorithms, like PDE-AIP, CII-NLM, DST, SSTV, JADE, and 2D-ABC adaptive filtering algorithm used for satellite image denoising, were also considered for comparison.

Experiments were conducted for denoising satellite images corrupted with additive white Gaussian noise of three different noise variance levels (i.e., 10%, 20%, and 30%). The quantitative and qualitative comparisons between different denoising algorithms revealed the efficiency of the proposed algorithm in preserving significant information bearing structures like edges. It also resulted in very less image artifacts with LMSE, particularly at high Gaussian noise variance levels. Convergence characteristics comparisons of the three recent metaheuristic-based algorithms used for image denoising also revealed the rapid convergence ability and computational efficiency of the proposed algorithm to converge to the least possible MSE value, within a fixed number of iterations. Statistical analysis along with the box-and-whisker plots also gave substantial evidence to prove the superiority of the 2D-CSAWF algorithm in handling real-time applications. One major advantage of the proposed denoising algorithm is that since the execution does not require transformation of signals to complex domains like Wavelet or Fourier transform, the computational complexity can be significantly reduced.

As a future study, the performance of the proposed algorithm can be evaluated for widespread 2-D signal processing applications, like system identification, channel estimation, etc.

Acknowledgment

The authors would like to thank the editors and anonymous reviewers for their valuable suggestions and comments which helped to improve the quality of this paper.

References

[1] X. Y. Wang, Y. C. Liu, and H. Y. Yang, "An efficient remote sensing image denoising method in extended discrete shearlet domain," *J. Math. Imag. Vis.*, vol. 49, no. 2, pp. 434–453, Jun. 2014.

[2] P. Liu, F. Huang, G. Li, and Z. Liu, "Remote-sensing image denoising using partial differential equations and auxiliary images as priors," *IEEE Geosci. Remote Sens. Lett.*, vol. 9, no. 3, pp. 358–362, May 2012.

[3] A. Pizurica, B. Huysmans, P. Scheunders, and W. Philips, "Wavelet domain denoising of multispectral remote sensing imagery adapted to the local spatial and spectral context," in *Proc. Int. Conf. Geosci. Remote Sens. Symp.*, Jul. 2005, vol. 6, pp. 4260–4263.

[4] J. Kang and W. Zhang, "Quickbird remote sensing image denoising using wavelet packet transform," in *Proc. 2nd Int. Symp. Intell. Inf. Technol. Appl.*, Dec. 2008, vol. 3, pp. 315–318.

[5] H. Taşmaz, H. Demirel, and G. Anbarjafari, "Satellite image enhancement by using dual tree complex wavelet transform: Denoising and illumination enhancement," in *Proc. 20th Signal Process. Commun. Appl. Conf.*, Apr. 2012, pp. 1–4.

[6] P. Ganesan and V. Rajini, "Segmentation and denoising of noisy satellite images based on modified fuzzy c-means clustering and discrete wavelet transform for information retrieval," *Int. J. Eng. Technol.*, vol. 5, no. 5, pp. 3858–3869, Oct. 2013.

[7] B. Xue, Y. Huang, J. Yang, L. Shi, Y. Zhan, and X. Cao, "Fast nonlocal remote sensing image denoising using cosine integral images," *IEEE Geosci. Remote Sens. Lett.*, vol. 10, no. 6, pp. 1309–1313, Nov. 2013.

[8] J. Yan and W. S. Lu, "Image denoising by generalized total variation regularization and least squares fidelity," *Multidimensional Syst. Signal Process.*, vol. 26, no. 1, pp. 243–266, Jan. 2015.

[9] S. Santhosh, N. Abinaya, G. Rashmi, V. Sowmya, and K. Soman, "A novel approach for denoising coloured remote sensing image using Legendre Fenchel transformation," in *Proc. Int. Conf. Recent Trends Inf. Technol.*, Apr. 2014, pp. 1–6.

[10] T. Anju and N. N. Raj, "Satellite image denoising using shearlet transform," in *Proc. Int. Conf. Commun. Signal Process.*, Apr. 2016, pp. 0571–0575.

[11] V. Soni, A. K. Bhandari, A. Kumar, and G. K. Singh, "Improved sub-band adaptive thresholding function for denoising of satellite image based on evolutionary algorithms," *IET Signal Process.*, vol. 7, no. 8, pp. 720–730, Oct. 2013.

[12] N. Peng, S. Sun, R. Wang, and P. Zhong, "Combining interior and exterior characteristics for remote sensing image denoising," *J. Appl. Remote Sens.*, vol. 10, no. 2, Apr. 2016, Art. no. 025016.

[13] A. K. Bhandari, D. Kumar, A. Kumar, and G. K. Singh, "Optimal sub-band adaptive thresholding based edge preserved satellite image denoising using adaptive differential evolution algorithm," *Neurocomputing*, vol. 174, pp. 698–721, Jan. 2016.

[14] H. K. Aggarwal and A. Majumdar, "Hyperspectral image denoising using spatio-spectral total variation," *IEEE Geosci. Remote Sens. Lett.*, vol. 13, no. 3, pp. 442–446, Mar. 2016.

[15] Z. Telatar, "Adaptive filter design for image deblurring by using multicriteria blurred image information," *Digit. Signal Process.*, vol. 15, no. 1, pp. 4–18, Jan. 2005.

[16] O. Kukrer and A. Hocanin, "Frequency-response-shaped LMS adaptive filter," *Digit. Signal Process.*, vol. 16, no. 6, pp. 855–869, Nov. 2006.

[17] Z. W. Li, X. L. Ding, D. W. Zheng, and C. Huang, "Least squares-based filter for remote sensing image noise reduction," *IEEE Trans. Geosci. Remote Sens.*, vol. 46, no. 7, pp. 2044–2049, Jul. 2008.

[18] M. M. Hadhoud and D. W. Thomas, "The two-dimensional adaptive LMS (TDLMS) algorithm," *IEEE Trans. Circuits Syst.*, vol. 35, no. 5, pp. 485–494, May 1988.

[19] M. Muneyasu, T. Hinamoto, and H. Yagi, "A realization of 2-D adaptive filters using affine projection algorithm," *J. Franklin Inst.*, vol. 335, no. 7, pp. 1185–1193, Sep. 1998.

[20] G. O. Glentis, "An efficient affine projection algorithm for 2-D FIR adaptive filtering and linear prediction," *Signal Process.*, vol. 86, no. 1, pp. 98–116, Jan. 2006.

[21] S. Haykin and B. Widrow, *Least-Mean-Square Adaptive Filters*. New York, NY, USA: Wiley, Sep. 2003, vol. 31.

[22] H. Zhang, A. Nosratinia, and R. Wells, "Image denoising via wavelet-domain spatially adaptive FIR wiener filtering," in *Proc. IEEE Int. Conf. Acoust., Speech, Signal Process.*, 2000, vol. 4, pp. 2179–2182.

[23] J. L. de Paiva, C. F. Toledo, and H. Pedrini, "An approach based on hybrid genetic algorithm applied to image denoising problem," *Appl. Soft Comput.*, vol. 46, pp. 778–791, Sep. 2016.

[24] M. Malik, F. Ahsan, and S. Mohsin, "Adaptive image denoising using cuckoo algorithm," *Soft Comput.*, vol. 20, no. 3, pp. 925–938, Mar. 2016.

[25] S. T. Tzeng, "Design of 2-D FIR digital filters with specified magnitude and group delay responses by GA approach," *Signal Process.*, vol. 87, no. 9, pp. 2036–2044, Sep. 2007.

[26] K. Boudjelaba, D. Chikouche, and F. Ros, "Evolutionary techniques for the synthesis of 2-D FIR filters," in *Proc. Statist. Signal Process. Workshop*, Jun. 2011, pp. 601–604.

[27] S. K. Sarangi, R. Panda, and M. Dash, "Design of 1-D and 2-D recursive filters using crossover bacterial foraging and cuckoo search techniques," *Eng. Appl. Artif. Intell.*, vol. 34, pp. 109–121, Sep. 2014.

[28] F. LatifoğLu, "A novel approach to speckle noise filtering based on artificial bee colony algorithm: An ultrasound image application," *Comput. Methods Programs Biomed.*, vol. 111, no. 3, pp. 561–569, Sep. 2013.

[29] S. Kockanat, N. Karaboga, and T. Koza, "Image denoising with 2-D FIR filter by using artificial bee colony algorithm," in *Proc. Int. Symp. Innov. Intell. Syst. Appl.*, Jul. 2012, pp. 1–4.

[30] S. Kockanat and N. Karaboga, "A novel 2D-ABC adaptive filter algorithm: A comparative study," *Digit. Signal Process.*, vol. 40, pp. 140–153, May 2015.

[31] R. C. Gonzalez and R. E. Woods, *Digital Image Processing*. Noida, India: Pearson Educ. India, Oct. 2008.

[32] J. S. Lee, "Digital image enhancement and noise filtering by use of local statistics," *IEEE Trans. Pattern Anal. Mach. Intell.*, vol. PAMI-2, no. 2, pp. 165–168, Mar. 1980.
[33] D. T. Kuan, A. A. Sawchuk, T. C. Strand, and P. Chavel, "Adaptive noise smoothing filter for images with signal-dependent noise," *IEEE Trans. Pattern Anal. Mach. Intell.*, vol. PAMI-7, no. 2, pp. 165–177, Mar. 1985.
[34] S. G. Chang, B. Yu, and M. Vetterli, "Image denoising via lossy compression and wavelet thresholding," in *Proc. Int. Conf. Image Process.*, Oct. 1997, vol. 1, pp. 604–607.
[35] S. G. Chang, B. Yu, and M. Vetterli, "Spatially adaptive wavelet thresholding with context modeling for image denoising," *IEEE Trans. Image Process.*, vol. 9, no. 9, pp. 1522–1531, Sep. 2000.
[36] X. S. Yang and S. Deb, "Cuckoo search via Lévy flights," in *Proc. World Congr. Nature Biol. Inspired Comput.*, Dec. 2009, pp. 210–214.
[37] S. Suresh and S. Lal, "An efficient cuckoo search algorithm based multilevel thresholding for segmentation of satellite images using different objective functions," *Expert Syst. Appl.*, vol. 58, pp. 184–209, Oct. 2016.
[38] H. Rakhshani and A. Rahati, "Snap-drift cuckoo search: A novel cuckoo search optimization algorithm," *Appl. Soft Comput.*, vol. 52, pp. 771–794, Mar. 2017.
[39] M. S. E. Abadi and S. N. Aali, "The novel two-dimensional adaptive filter algorithms with the performance analysis," *Signal Process.*, vol. 103, pp. 348–366, Mar. 2014.
[40] A. Hore and D. Ziou, "Image quality metrics: PSNR vs. SSIM," in *Proc. 20th Int. Conf. Pattern Recognit.*, Aug. 2010, pp. 2366–2369.
[41] Q. Huynh-Thu and M. Ghanbari, "Scope of validity of PSNR in image/video quality assessment," *Electron. Lett.*, vol. 44, no. 13, pp. 800–801, Jun. 2008.
[42] L. Zhang, L. Zhang, X. Mou, and D. Zhang, "FSIM: A feature similarity index for image quality assessment," *IEEE Trans. Image Process.*, vol. 20, no. 8, pp. 2378–2386, Aug. 2011.
[43] Z. Wang and A. C. Bovik, "A universal image quality index," *IEEE Signal Process. Lett.*, vol. 9, no. 3, pp. 81–84, Sep. 2002.
[44] C. P. Loizou, C. S. Pattichis, M. Pantziaris, T. Tyllis, and A. Nicolaides, "Quality evaluation of ultrasound imaging in the carotid artery based on normalization and speckle reduction filtering," *Med. Biol. Eng. Comput.*, vol. 44, no. 5, pp. 414–426, May 2006.

Shilpa Suresh (S'17) received the M.E. degree in communication systems from the Hindustan University, Chennai, India, in 2012, and is currently working toward the Ph.D. degree in satellite image processing from the National Institute of Technology, Karnataka, Mangaluru, India.

Her research interest focuses on satellite image processing using stochastic metaheuristic algorithms.

Shyam Lal (M'11) received the M.Tech. degree in electronics and communication engineering from the National Institute of Technology, Kurukshetra, Kurukshetra, India, in 2007, and the Ph.D. degree in image processing from the Birla Institute of Technology, Mesra, Ranchi, India, in 2013.

He is an Assistant Professor in the Department of Electronics & Communication Engineering, National Institute of Technology Karnataka, Mangalore, India. His research interests include digital image processing, remote sensing, and medical image processing.